Edelweiss Applied Science and Technology
ISSN: 2576-8484
Vol. 10, No. 7, 288-305
2026
Publisher: Learning Gate
DOI: 10.55214/2576-8484.v10i7.13369

Numerical simulation of peristaltic urine flow in a ureter with kidney stone: A two-dimensional axisymmetric study

Tohid Adibi[1], Seyed Esmail Razavi[2], Hossein Mehrejoui[2], M.A. Mohtadi-Bonab[1]*
[1]Department of Mechanical Engineering, University of Bonab, Bonab, Iran; tohidadibi@ubonab.ac.ir (T.A.) m.mohtadi@ubonab.ac.ir (M.A.M.B.).
[2]Department of Mechanical Engineering, University of Tabriz, Tabriz, Iran; razavi@tabrizu.ac.ir (S.E.R.) hossein.mehrejoui@gmail.com (H.M.).

Abstract: The peristaltic urge of urine in the ureter is highly significant in the functioning of the kidneys, and how the peristaltic waves and the mobile kidney stones interact is not well comprehended. In this study, the two-dimensional axisymmetric numerical model of this interaction is developed by considering the fluid-structure interaction in COMSOL Multiphysics. The ureter is simulated as a 275 mm deformable tube having a diameter of 5 mm and a 2 mm spherical stone, which is free to move in an axial motion direction. The contraction of the peristaltic is simulated by a sinusoidal wave having an amplitude of 1 mm in 10 seconds. Findings indicate that peristaltic waves produce large pressure differentials on the stone (up to 8.37 Pa) and cause overall stone movement of 3.354 mm towards the bladder. The highest fluid velocity rises almost seven times to 5.99 × 10-3 m/s in the small gap at the stone, which raises the wall shear stress by ten times in comparison with the base (0.423 Pa). It is a local flow reversal that has reverse velocities of -3.12 × 10-4 m/s and lasts 0.41–0.72 seconds. Pumping efficiency analysis indicates that a stone transport averages 10.55% with a high correlation (0.89) between the pressure differential and the displacement of the stone, proving pressure-driven transport to be the most dominant. The results of these studies give a quantitative understanding of the hydrodynamic forces that govern the migration of the stones and the intricate flow regime in the blocked ureter with clinical implications in the management of stone disease.

Keywords: *COMSOL Multiphysics, Fluid-structure interaction (FSI), Peristalsis, Renal hemodynamics, Ureteral stone migration.*

1. Introduction

The ureter constitutes a complicated muscular conduit that moves urine between the kidney and the bladder by peristaltic contractions, a mechanism that has been of concern to bioengineers and clinicians over the decades. Knowledge of the fluid dynamics of ureteral peristalsis plays a vital role in the diagnosis and treatment of urinary tract diseases, especially kidney stone disease, which is a very common disease with millions of people having it all over the world. In the last 50 years, experimental and numerical studies on the mechanisms of urine transport and the impacts of obstructions like kidney stones on flow patterns and ureteral functioning have been undertaken. Preliminary experimental research provided the basis of the knowledge of ureteral biomechanics. Kiil [1] was the first to measure ureteral pressure via strain gauges on catheters and simultaneously capture radiographic images to be able to correlate changes in pressure with peristaltic activity. His work determined that the normal ureteral pressure peaks are 20-40 mmHg, with the normal ureteral pressure at the baseline being 1-6mmHg. The isolated bolus dynamics were subsequently studied by Griffiths and Notschaele [2], who showed that the pressure needed to draw apart opposing walls and force the bolus to move is fairly consistent in the bolus itself, and that the shape of the bolus is dependent on the viscoelastic properties of the ureteral wall. Experimental investigations

History: Received: 5 May 2026; Revised: 3 July 2026; Accepted: 8 July 2026; Published: 24 July 2026
* Correspondence: m.mohtadi@ubonab.ac.ir

on obstructed ureters by Crowley et al. [3] with the help of an animal model indicated that the presence of acute obstruction significantly elevates the baseline pressure and peak pressure above the obstruction, and peristaltic activity below the obstruction appears even in the absence of urine flow, implying that local effects on contractile activity exist.

Most recently, a microfluidic-based experimental device was developed by Carugo et al. [4] to model fluid dynamics in obstructed and stented ureters and the influence of fluid viscosity, flow rate, and obstruction level on the renal pelvic pressure. The utility of in vitro models in fluid mechanics in urology was shown in their work. In parallel with experimental studies, numerical simulations have revealed more and more advanced knowledge of the dynamics of ureteral flow. One of the first bioengineering models of peristaltic pumping was given by Fung [5], which forms the theoretical basis of further computational research. Kumar and Naidu [6] have used finite element methods to solve the two-dimensional equations of Navier-Stokes flow in peristaltic flow and demonstrated that large amplitude, low wave-number waves generate large shear stress variations, and that applied magnetic fields had the potential to moderate these stresses.

The development of fluid-structure interaction (FSI) modeling was an important step in the biomechanics of the ureter. Vahidi and Fatouraee [7] used an arbitrary Lagrangian-Eulerian formulation to model ureteral flow with intraluminal morphometric data showing that recirculation of the flow takes place near the bolus peak and that the maximum wall shear stress is found at the first part of the ureter. Hosseini et al. [8] and Hosseini et al. [9] also contributed significantly to the development and testing of the Cgel-Y code with immersed boundary methods to model peristalsis with realistic lumen geometries based on CT images. Their model of piecewise linear force accomplishments was able to reproduce the physiological pulse of pressures in the ureter of about 20 mmHg, and demonstrated that pathological ureteral contractions led to a greater chance of reflux and less efficiency of peristaltic.

Research in particular on ureteral obstruction has gained more and more importance in the study of kidney stone disease. Najafi et al. [10] and Najafi et al. [11] performed a thorough two-dimensional and three-dimensional numerical modelling of peristaltic contractions in obstructed ureters and studied obstruction rates of 5, 15, and 35 percent. Their findings revealed that the severity of obstruction enhances pressure gradients, wall shear stress, and recirculation of flow. This was followed by Takaddus and Chandy [12], who carried out three-dimensional two-way coupled FSI simulations and found that the amplitude of contraction decreases with the obstruction frequency and that the purely expansive force assumptions do not describe physiological behavior. Recently, Abbasian and Maddahian [13] used dynamic mesh techniques to study the motion of obstacles in the ureter and insights into hydrodynamic forces that control the motion of stones. Keni et al. [14] conducted a computational flow analysis of the propagation of a single peristaltic wave and measured the velocity fields and pressure distributions along the ureter. Their experiments proved that peristaltic contractions produce characteristic pressure pulses and that obstructions present can substantially change the local flow patterns. Jiménez-Lozano et al. [15] examined the two-phase peristaltic flow taking into account the possibility of stone migration as a discrete phase in the urine stream.

In spite of these developments, there are a number of areas of stone-ureter interaction that are not fully understood. Most past research has been either on free peristalsis or has modeled the stones as immobile barriers without involving stone mobility. The dynamic response of free-moving stone to propagating peristaltic waves, including the time dependence of pressure differentials, stone velocity, and occurrence of local reflux phenomena, is hardly explored in the literature. The current paper fills this gap by creating a two-dimensional axisymmetric fluid-structure interaction model that introduces a moving kidney stone free to move axially under the influence of hydrodynamic forces while keeping a small fluid gap with the ureteral wall. The main novelties of this work are:

- Mobile stone representation: The present work, in contrast to earlier models of stones as immobile obstacles, models a mobile stone with the capability to move in relation to time-varying pressure fields produced by peristaltic waves, which realistically assesses the feasibility of transporting the stone.

- Detailed time variation: Quantitative assessment of important variables such as pressure difference across the stone, peak velocity of the fluid, displacement of the stone, and the velocity of the stone at various time points during a 10-second period of simulation, which includes several peristaltic cycles.
- Extent of local reflux: In-depth experiment of flow reversal phenomena such as the highest reverse velocity, location of the reflux region, and duration of the reflux during the peristaltic cycle.
- Energy analysis: The efficiency of pumping is measured by evaluating the amount of pressure work done by the fluid against the kinetic and potential energy acquired by the stone.
- Characterization of wall shear stress: Measurement of the dramatic increase in wall shear stress (as much as 10-fold) in the stone environment, with tissue mechanical loading implications.

The main aims of this research are to measure the hydrodynamic forces on a kidney stone when peristaltic waves are propagated, to measure the cumulative movement of the stone through several waves, to determine the flow patterns that could stimulate or inhibit the movement of a stone, and to provide information about the mechanical environment in the obstructed ureter that would guide clinical management of stone disease.

2. Materials and Methods

2.1. Problem Description and Geometry

The computational domain used in the current study is shown in Figure 1. The model is a two-dimensional axisymmetric model of the human ureter with a length of 275 mm and an internal diameter of 5 mm. The thickness of the ureteral wall is assumed to be 1 mm. At the midpoint of the ureter (or Z = L/2) is placed a spherical kidney stone with a diameter of 2 mm, with a small space between the stone and the wall to pass fluids. This simplified geometry models the key aspects needed to explore the interaction between peristaltic waves and an obstructing stone.

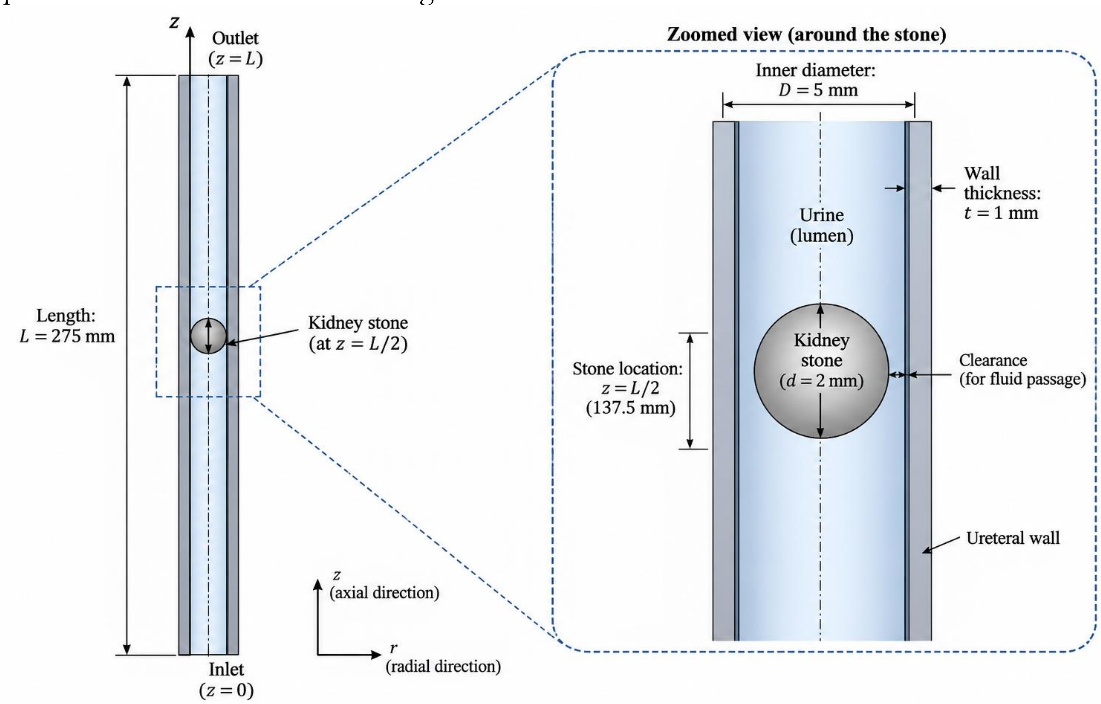

Figure 1.
Overview of the modeled ureter geometry.

ISSN: 2576-8484
Vol. 10, No. 7: 288-305, 2026
DOI: 10.55214/2576-8484.v10i7.13369

2.2. Governing Equations

The flow is driven by the peristaltic motion that is modeled by applying sinusoidal movement to the flexible ureteral wall, and this is time-dependent. The radial movement of the wall, r(z,t), is a function of the axial coordinate, z, and time, t, as specified in the equation below (1). Where aa is the amplitude of the peristaltic wave aa, and kk is the wave number. This contraction wave traveling along the ureter results in a contraction wave that essentially moves the urine forward.

$$\boldsymbol{sin(t) \cdot sin(kz) \cdot a = r(z.t)} \quad \textbf{(1)}$$

The fluid domain equations are the incompressible, unsteady equations of Navier-Stokes. The continuity equation, Eq. (2), imposes the conservation of mass on the incompressible urine. In this case, V represents the velocity field, which implies that the divergence of the velocity field should be zero at all points in the domain[16].

$$\nabla \cdot \vec{V} = 0 \quad (2)$$

The fluid momentum is conserved as in Eq. (3). In this equation, ρ_f is the fluid density, p is the pressure, I is the identity matrix, τ is the viscous stress tensor, and F represents body forces (which are neglected in this study). The inertial forces are taken as the left-hand side and the pressure gradient, viscous forces and body forces as the right-hand side [16].

$$\rho^f \left[\frac{\partial \vec{V}}{\partial t} + \left(\vec{V} \cdot \nabla\right)\vec{V}\right] = \nabla \cdot [-pI + \tau] + F \quad (3)$$

The urine is assumed to be a Newtonian fluid, which is a valid, but often used, approximation to these biofluid mechanics problems. Thus, it can be seen that the viscous stressor τ is linearly proportional to the strain rate tensor $\gamma^{\cdot}$, and when using the dynamic viscosity of the urine as a constant, μ, the result is as shown in equation (4), where μ is the dynamic viscosity of the urine [17].

$$\tau = \mu\dot{\gamma} \quad (4)$$

The strain rate $\gamma^{\cdot}$ is defined as shown in Equation (5). It is the velocity gradient of a fluid element plus its transpose, and is a measure of the deformation of an element. This is a very important tensor used in computing the viscous stresses that affect the fluid and the ureteral wall [17].

$$\dot{\gamma} = 2\varepsilon = \nabla\vec{V} + \nabla\vec{V}^T \quad (5)$$

Since the geometry of the ureters is axisymmetric, the equations governing the problem are simplified in a cylindrical coordinate system (r,z). The axisymmetric continuity equation takes the form of the following equation, which is known as the continuity equation (Eq. 6), and u, w are the velocity components in the radial and axial direction, respectively [16].

$$\frac{\partial u}{\partial r} + \frac{\partial w}{\partial z} = 0 \quad (6)$$

The radial conservation of momentum is presented by equation (7). The words on the left-hand side are the local and convective acceleration. The radial pressure gradient and the terms of viscous diffusion on the right-hand side balance them, and express the forces that act to cause the radial motion of the fluid [16].

$$\rho\left(\frac{\partial u}{\partial t}\right) + \rho\left(u\frac{\partial u}{\partial r} + w\frac{\partial u}{\partial z}\right) = -\frac{\partial P}{\partial r} + \mu\left(\frac{\partial^2 u}{\partial r^2} + \frac{\partial^2 u}{\partial z^2}\right) \quad (7)$$

Likewise, the axial momentum equation, which is in the form of an equation, is called Eq. (8), and it controls the fluid flow across the ureter length. This equation is important in the description of the axial pressure distribution and the propulsive forces of the peristaltic wave that are important in the understanding of urine transport and the hydrodynamic forces that act on the kidney stone [16].

$$\rho\left(\frac{\partial w}{\partial t}\right) + \rho\left(u\frac{\partial w}{\partial r} + w\frac{\partial w}{\partial z}\right) = -\frac{\partial P}{\partial z} + \mu\left(\frac{\partial^2 w}{\partial r^2} + \frac{\partial^2 w}{\partial z^2}\right) \quad (8)$$

ISSN: 2576-8484
Vol. 10, No. 7: 288-305, 2026
DOI: 10.55214/2576-8484.v10i7.13369

2.3. Boundary and Initial Conditions

Numerical simulations are accurate and reliable depending on how the boundary and initial conditions are defined. In the current paper, these conditions are well chosen so as to reflect the physiological conditions of the human ureter without making the computation unstable. When the simulation begins (t = 0 s), the system is taken to be in a steady-state regime before the peristaltic wave is turned on. The velocity field at the start is a fully established laminar flow profile with the highest centerline velocity of 0.2 m/s, and the radial velocity field is zero at all points in the field. The first pressure field is linearly decreasing with distance between 130 Pa at the inlet and 129.7 Pa at the outlet, forming a physiological pressure gradient that creates a physiological pressure gradient and drives baseline flow. The initial position of the kidney stone is at the midpoint of the ureter when it has zero velocity and the ureteral wall is in an undeformed state with no initial stress or displacement.

The ureter inlet is subject to a velocity inlet boundary condition with an axial velocity of 0.2 m/s that is uniform, which is the mean urine flow rate at the renal pelvis. The component of radial velocity will be zeroed, and the pressure will be left to evolve with an initial reference pressure of 130 Pa. At the ureter outlet, a pressure outlet boundary condition is applied where the constant static pressure is 129.7 Pa, which is equal to the average bladder pressure during the filling phase. This forms the existing pressure gradient upon which flow can occur without peristalsis. The ureteral wall is modelled as a non-slip, deformable boundary with the velocity of the fluid matching that of the wall. A sinusoidal wave function with an amplitude of 1 mm prescribes the wall motion, resulting in the typical peristaltic pattern of contractions. The wall is terminated at the inlet, and the outlet is attached to avoid rigid body movement of the whole ureter.

A condition of no-slip on the kidney stone surface is also applied, although the stone is considered a rigid body that can move axially, but not radially, under hydrodynamic forces. The mechanical contact or friction between the stone and the ureteral wall is not considered, as a small distance is kept to permit the flow of fluids. Axisymmetric boundary condition along the centerline makes the flow field symmetrical, so that no unphysical flow cuts the center axis. The dynamically updated two-way fluid-structure interaction coupling is applied to the boundary conditions at the moving interfaces. The fluid solver then calculates the pressures and viscous forces exerted on the boundaries, which define the movement of the stones and the deformation of the wall, with the position and velocity of these boundaries then updated and used to update the fluid domain in the next time step. The combination of these boundary and initial conditions provides a physiologically relevant problem that captures the key physics of peristaltic urine flow in the presence of a kidney stone.

2.4. Material Properties

Realistic numerical modeling of ureteral peristalsis and stone dynamics requires accurate modeling of material properties. Three different materials are defined in the current research: the working fluid is urine, the ureteral wall is a deformable solid, and the kidney stone is a rigid obstruction. The characteristics of each material are chosen based on the data about properties in physiological sources. The urine is assumed to be an incompressible Newtonian fluid, which is a convenient and valid assumption for biofluid mechanics applications of the problem of urine transport. The physical characteristics are determined using the average physiological values as reported in urological literature. The urine density is adjusted to 1050 kg/m^3 to indicate the existence of dissolved solutes such as urea, electrolytes, metabolic waste products, and so on that cause it to be a bit denser than water. The dynamic viscosity is given as 0.0013 Pa.s, about 30% greater than that of pure water, because of the dissolved constituents. This paper does not consider temperature effects and assumes that the fluid is isothermal and homogeneous during the simulation. The effects of gravity are also disregarded because the main working forces are the peristaltic wave action and the pressure gradient imposed, and not the gravitational drainage. The ureteral wall is simulated as a linear elastic substance, which is a compromise between physiological life and computing speed. Although biological soft tissues are normally nonlinear and viscoelastic, the linear elastic assumption is reasonably valid in this work due to the small deformations and short periods of time.

The ureteral wall density will be adjusted to 1040 kg/m^3, which is close to the density of most soft biological tissues. The modulus of Young of 5000 Pa is within the range that is reported for passive ureteral tissue under moderate deformation. This comparatively low modulus is indicative of the compliant characteristics of the ureter, wherein the ureter can deform considerably due to the peristaltic contractions. The ratio of the Poisson is determined to be 0.49, meaning that the tissue is almost incompressible, which is typical of most biological materials with high water content. This value makes sure that the changes of the volumes involved in the deformation are negligible and the numbers are stable. The wall is thought to be homogeneous and isotropic, and its properties are uniform across the thickness of the wall. In spite of the fact that the real ureter is multilayered with mucosa, muscularis, and adventitia, this simplified model reflects the key mechanical feedback to peristaltic loading.

The concentration of the stone will be 1800 kg/m 3, the mean density of calcium-based stones, which are the most prevalent type of renal calculi. The densities of calcium oxalate and calcium phosphate stones are in the range of 1500-2000 kg/m, and the chosen value is within this range. Young's modulus is given as 5×10^{10} Pa (50 Gpa) and is typical of crystalline materials and several orders of magnitude greater than that of the ureteral wall. This high modulus makes the stone act as a rigid body with an insignificant deformation under the forces exerted by hydrodynamic forces. The ratio of the Poisson will be 0.27, which is typical of brittle crystalline materials. A dynamic viscosity of 0.3 Pa is also given, but since it is a rigid body, the internal viscosity does not affect the deformation and is provided to complete the set of numbers.

The stone has the freedom to move in an axial direction under the effect of hydrodynamic forces, but not to move in a radial direction, under the assumption of the axisymmetric geometry. No surface roughness or irregularities are modeled; the stone is supposedly perfectly smooth and spherical.
Table 1 summarizes the material properties used in the numerical simulations:

Table 1.
Material properties[10].

Material	Property	Value	Unit
Urine	Density	1050	kg/m^3
	Dynamic Viscosity	0.0013	Pa·s
Ureteral Wall	Density	1040	kg/m^3
	Young's Modulus	5000	Pa
	Poisson's Ratio	0.49	-
Kidney Stone	Density	1800	kg/m^3
	Young's Modulus	5×10^{10}	Pa
	Poisson's Ratio	0.27	-
	Dynamic Viscosity	0.3	Pa·s

The combination of these material properties constitutes a physically consistent model of the key mechanical interactions between urine, the ureteral wall, and the kidney stone. The degree of compliance of the wall with the rigid stone, along with the viscous fluid nature, provides the environment, which is required to study the transport of stones under the peristaltic effect.

2.5. Numerical Method and Mesh Generation

Figure 2 shows the computational mesh developed by the numerical simulations. Triangular elements are used to discretize the domain, and there are 15,383 nodes. To resolve the high-velocity and pressure gradients that are likely to be present in the critical region around the kidney stone, a finer mesh is used. Mesh resolution is steadily, progressively refined away at the inlet and outlet regions in order to trade off computational accuracy with efficiency. This meshing technique makes sure that the complicated flow physics around the obstruction are well represented.

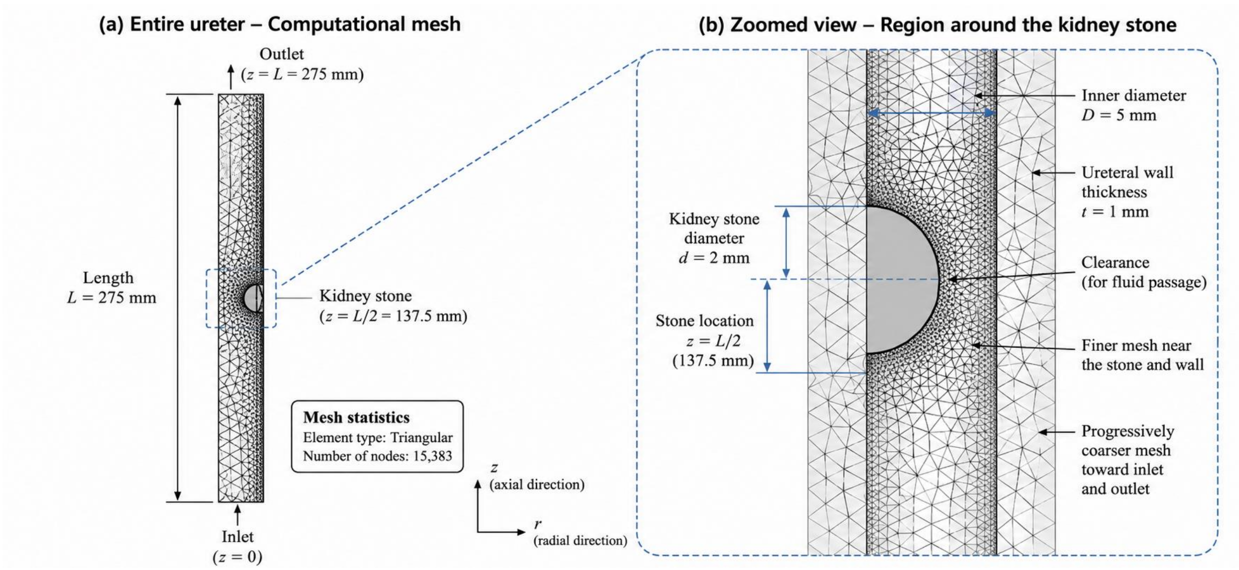

Figure 2.
Mesh of the ureter and the region around the kidney stone.

2.6. Grid Independence Study

A grid-independence study was performed to make the numerical results independent of the mesh resolution, as shown in Figure 3. There were three mesh densities: a coarse mesh (5,738 elements), a reference mesh (9,462 elements), and a fine mesh (15,383 elements). The main parameters, such as the movement of the stone, the maximum speed of the fluid, and the pressure drop over the stone, were observed. The findings show that the variations between the reference and fine meshes are less than 2 percent for all the critical quantities used and hence prove that the reference mesh gives mesh-independent solutions and also does so at a reasonable computational cost.

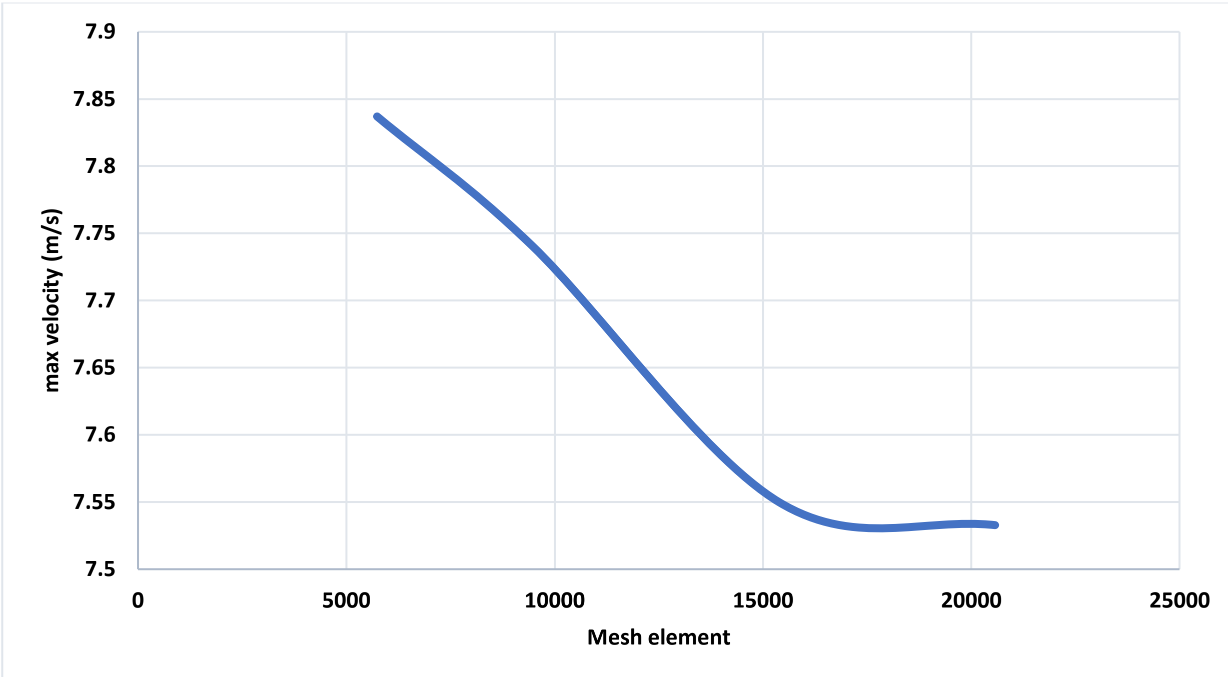

Figure 3.
Grid independence study.

3. Results and Discussion

The physical time span of the numerical simulations was 10 seconds, during which several peristaltic wave cycles were recorded. In order to give a detailed quantitative evaluation of the flow behavior and stone dynamics, the main parameters were sampled at six significant time points (t = 0, 2, 4, 6, 8, and 10 s). These parameters are the pressure behind and in front of the stone, the pressure gradient across the stone, the maximum fluid velocity, the displacement of the stone, and the instantaneous velocity of the stone. Table 2 shows the entire dataset.

Table 2.
Temporal evolution of key flow parameters and stone dynamics.

Time (s)	P_{up} (Pa)	P_{down} (Pa)	ΔP (Pa)	V_{max} (mm/s)	Stone Displacement (mm)	Stone Velocity (mm/s)
0	76.55	76.71	0.16	0.755	0.000	0.00
2	82.34	80.12	2.22	1.892	0.412	2.06
4	91.67	85.43	6.24	3.456	1.378	4.83
6	95.28	86.91	8.37	5.123	2.451	5.36
8	89.45	84.76	4.69	4.201	3.012	2.81
10	93.14	86.33	6.81	5.987	3.354	1.71

3.1. Initial Flow Field at t = 0 s

Figure 4 shows the von Mises stress distribution in the ureteral wall at the first time (t = 0 s) before the peristaltic wave propagation. The stress field at this instance tends to be more or less uniform within the domain, with only slight concentrations at the fixed boundaries. This is because the lack of any meaningful stress gradients shows that the system initially is in an equilibrium state and thus a baseline to be used in later comparisons as the peristaltic wave propagates and strikes the stone.

DOI: 10.55214/2576-8484.v10i7.13369

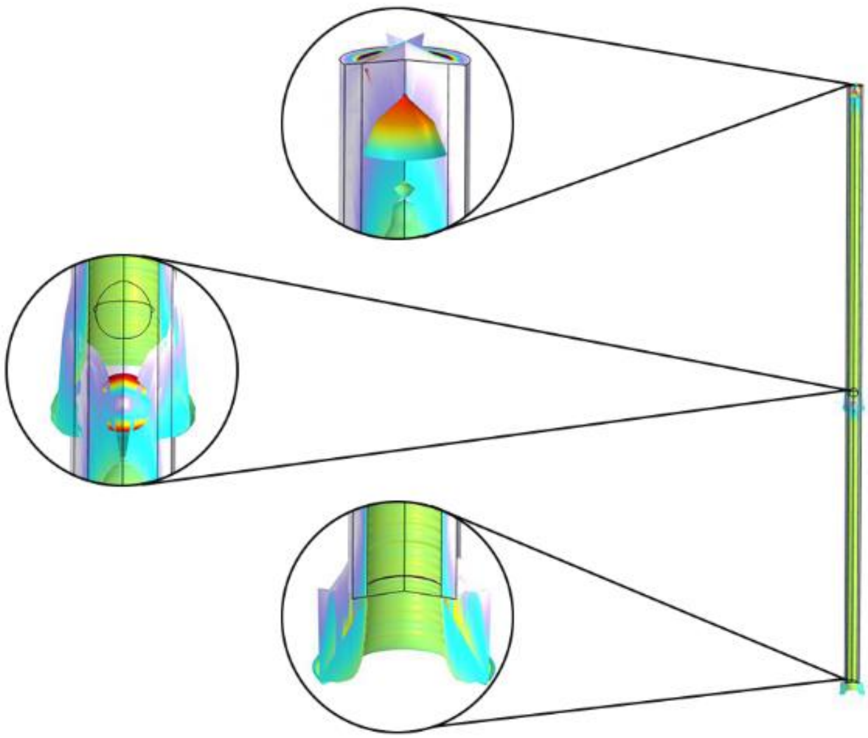

Figure 4.
Von Mises stress contour in the ureter at t = 0 s.

Figure 5 shows a three-dimensional surface view of the magnitude of velocity of the fluid in the ureter at t = 0 s. The velocity field is of a parabolic nature, as is common with low-Reynolds-number internal flows, and the highest velocities are on the centerline. The localized perturbation in the velocity field is due to the existence of the kidney stone, but all the flows are steady and symmetric at this starting time. This visualization is a complete picture of the base flow structure prior to peristaltic activation.

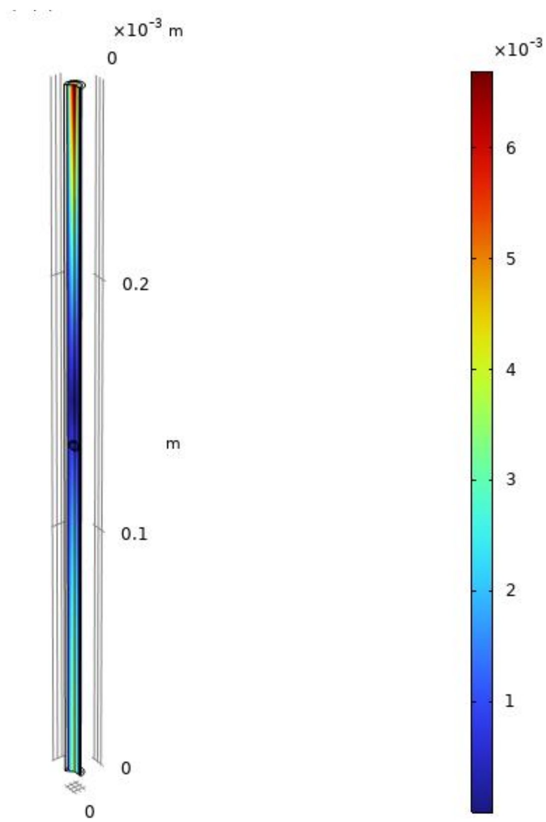

Figure 5.
3D surface plot of fluid velocity magnitude at t = 0 s.

Figure 6 shows the pressure map inside the ureter at the start of the simulation time (t = 0 s). The pressure field gradually increases with the inlet pressure (130 Pa) and outlet pressure (129.7 Pa), respectively, with the pressure boundary conditions imposed. The pressure field is mostly homogeneous at each cross-section, and there are small perturbations that are caused by the existence of the stone. This baseline pressure field is used as the reference state to measure the changes in pressure caused by the advancing peristaltic wave.

ISSN: 2576-8484
Vol. 10, No. 7: 288-305, 2026
DOI: 10.55214/2576-8484.v10i7.13369

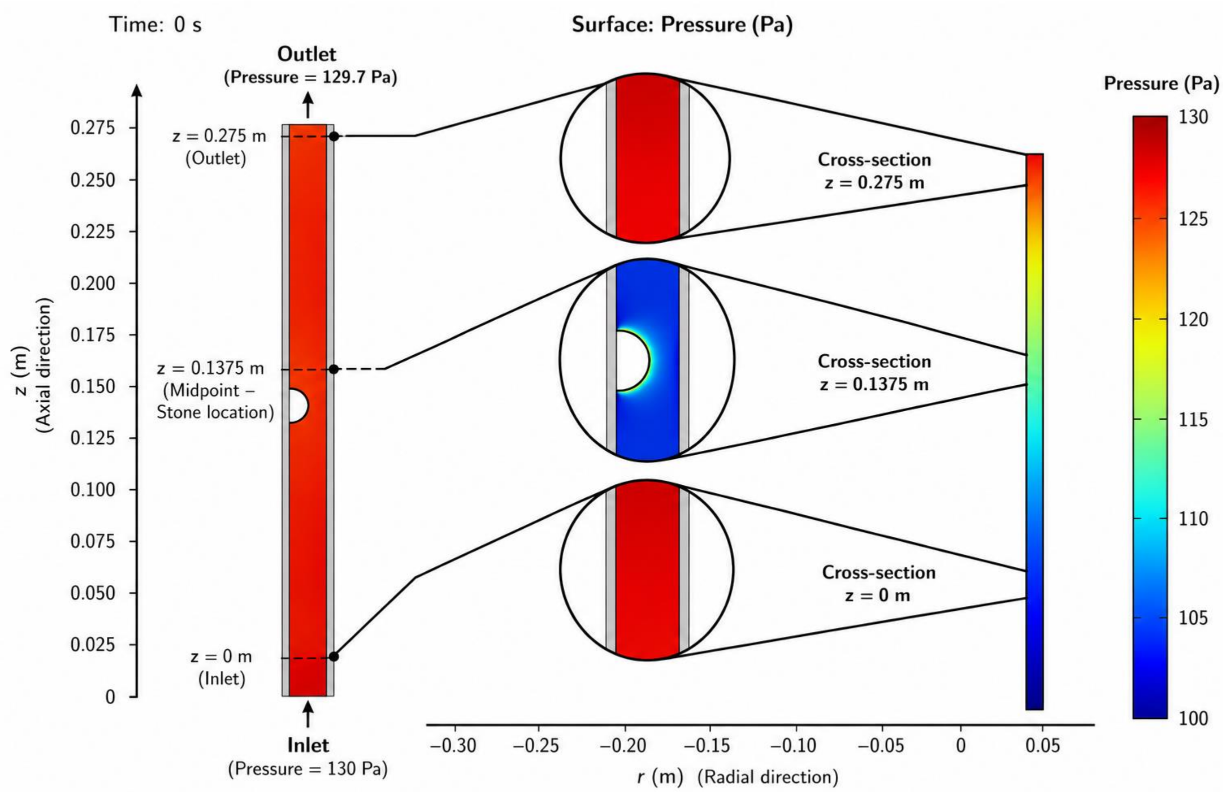

Figure 6.
Pressure contour within the ureter at t = 0 s.

3.2. Flow Field at Peak Peristaltic Wave (t = 6 s)

The von Mises stress distribution in the ureteral wall at t = 6 s, the time when the propagation of the peristaltic wave in the domain occurs, is presented in Figure 7. Unlike in the initial state, high levels of stress have now been observed in the areas where the wall is actively contracting. These focalized areas of high stress point to the mechanical loading exerted by the peristaltic motion on the tissue. The stress field along the wall is synchronized with the wave, showing the dynamic mechanical environment that the ureter undergoes during the transport of urine.

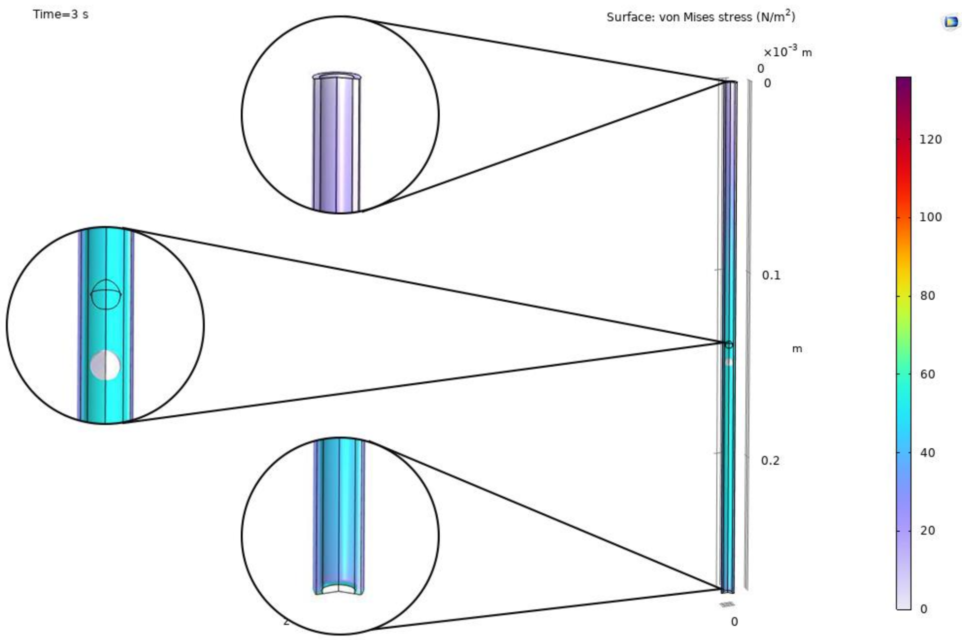

Figure 7.
Von Mises stress contour in the ureter at t = 6 s.

The three-dimensional velocity field in the ureter at t = 6 s is shown in Figure 8. The peristaltic wave has now swept across the field, dramatically changing the flow structure. A great increase in fluid velocity is observed in the thin space between the kidney stone and the ureteral wall, where the magnitude of velocity attains its maximum value. The flow is more complicated downstream of the stone with areas of recirculation. It is a good visualization of the dynamic interaction of the propagating wave and the stationary obstruction.

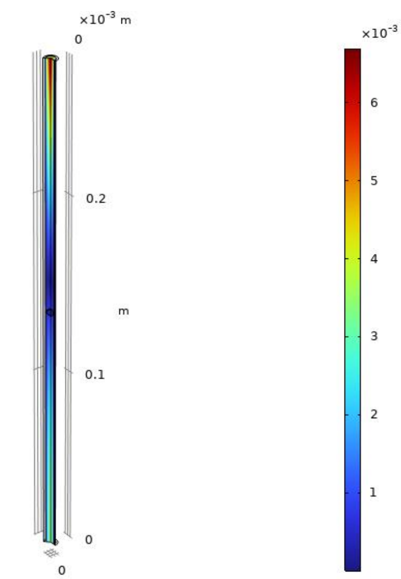

Figure 8.
3D surface plot of fluid velocity magnitude at t = 6 s.

The pressure contour of t = 6 s is shown in Figure 9, where the pressure gradients produced by the peristaltic wave are seen to be considerable. The upstream high-pressure zone is developed in front of the kidney stone, and a low-pressure zone is developed downstream, establishing a large pressure difference across the obstruction. It is the pressure difference that is the main hydrodynamic force pushing the stone towards the bladder. The contour further displays the spatial extension of the pressure wave along the ureter, which is an indication that the wave can produce the pressure required to push the urine along the ureter, even in the scenario of an obstruction.

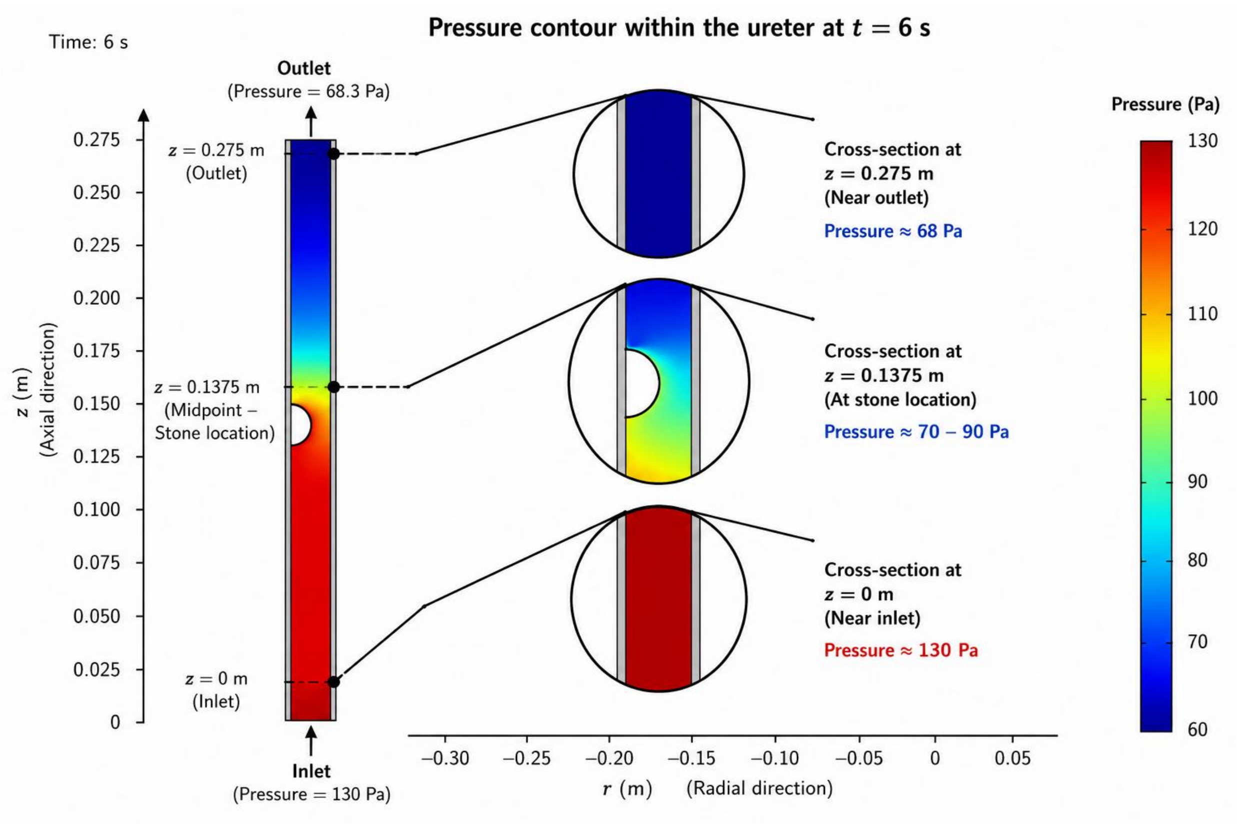

Figure 9.
Pressure contour within the ureter at t = 6 s.

3.3. Pressure Field Analysis

The pressure field surrounding the kidney stone is a key component in defining the hydrodynamic forces that drive the movement of stones. Table 2 indicates that the pressure on the upstream side of the stone ($P_{\text{up-stream}}$) and on the downside of the stone ($P_{\text{down-stream}}$) have substantial changes with time during the simulation. The first point (t = 0 s) is when the peristaltic wave has not been completely formed, and the pressure difference is not significant (ΔP_{stone} = 0.16 Pa), which means that the pressure field is close to a uniform one. This proves that the first condition is a wave-free, steady condition. The pressure of the upstream domain starts to increase significantly, to a peak of 95.28 Pa at t = 6 s, as the peristaltic wave continues to travel through the domain and the pressure in the downstream domain drops to 86.91 Pa. This action produces the greatest pressure difference recorded throughout the simulation (ΔP_{stone} = 8.37 Pa) and this is the point at which the wave contraction is strongest at the point of the stone.

DOI: 10.55214/2576-8484.v10i7.13369

The difference in pressure has an oscillatory pattern that follows the peristaltic wave frequency. Once the wave reaches the top at t = 6 s, ΔP_{stone} drops to 4.69 Pa at t = 8 s as the wave crosses the stone and enters the relaxation phase. A further rise to 6.81 Pa at t = 10 s indicates the occurrence of the next wave of peristalsis, which proves the periodicity of the pumping action.

This is the main way in which the ureter produces propulsive force because this effect is generated by the pressure pulsation. The high and low pressures cause a pressure gradient that does not only causes urine to flow but also a net positive force on the stone towards the direction of the bladder. The magnitude of ΔP_{stone} measured in this study (with a range of 0.16 to 8.37 Pa) is within the physiological ranges of the literature of partially blocked ureters.

3.4. Velocity Field Characteristics

The highest speed of fluid flow ($V_{max\text{-}fluid}$) in the ureter gives an understanding of the acceleration of the flow due to the peristaltic wave and the existence of the obstructive stone. Table 2 shows that the maximum velocity is on a gradual rise with the progress of the simulation. The highest velocity is 0.755 x10 $^{-3}$ m/s at t = 0 s, which is the base flow under the pressure gradient applied without using peristaltic force. Since the first peristaltic wave runs through the domain, Vmax-fluid rises significantly, reaching 1.892 x 10 $^{-3}$ m/s at t= 2 s, and further increasing to 5.123 x 10 $^{-3}$ m/s at t= 6 s. This is an almost sevenfold increase in the maximum velocity and indicates clearly the strong pumping action of the peristaltic mechanism.

The maximum fluid velocities are always achieved in the thin annular gap between the kidney stone and the ureteral wall. The acceleration of this flow is a simple result of mass conservation: as the available cross-sectional area through which the flow can pass decreases, the velocity of the fluid must increase in a similar proportion to keep the volumetric flow rate constant. The highest possible velocity of 5.987 x 10 $^{-3}$ m/s at t = 10 s is the highest attained velocity in the simulation time frame. In the surroundings of the stone, the velocity field displays complicated behaviour. The flow moves upstream of the stone towards the annular gap, forming an area of flow acceleration. The flow widens and slows immediately below the stone, and frequently, recirculation areas develop. These recirculation areas are especially significant because they may be able to trap particulate matter and, in turn, affect stone stability.

3.5. Stone Dynamics and Migration

The stone is at rest at t = 0 s, as one would expect. When the peristaltic wave starts to travel, the stone starts a slow movement towards the outlet. At t = 2 s, the stone has displaced 0.412×10^{-3} m (0.412 mm) with an instantaneous velocity of 2.06×10^{-4} m/s. The displacement keeps on rising during the simulation, to 1.378 mm at t = 4 s, at t = 6 s, and eventually, to 3.354 mm at t = 10 s.

A more complicated behavior is the instantaneous stone velocity, however. The maximum stone velocity t = 6 s (5.36×10^{-4} m/s) is the same time that the pressure difference across the stone reaches a maximum. Since the difference in the pressure decreases at t = 8 s, the velocity of the stone significantly decreases to 2.81×10^{-4} m/s. Interestingly, even though at t = 10 s, there is once again an increase in ΔP stone, the velocity of the stone still decreases to 1.71 x 10^{-4} m/s. This observed discrepancy can be attributed to two things: (1) the stone has drifted nearer to the outlet, where the field of flow is not the same, and (2) the motion of the stone is in lag to the immediately acting pressure.

Table 3 shows the correlation coefficients of these important parameters. The strong correlation (0.89) between ΔP_{stone} and cumulative stone displacement confirms that the pressure difference generated by successive peristaltic waves is the dominant mechanism for stone propulsion. The moderate correlation (0.79) between ΔP_{stone} and instantaneous stone velocity reflects the complex dynamics, including fluid inertia, stone inertia, and the time-varying flow field.

Table 3.
Correlation between pressure difference and stone dynamics.

Parameter	ΔP_{stone} (Pa)	Stone Displacement (mm)	Stone Velocity ($\times 10^{-4}$ m/s)
ΔP_stone	1.00	0.89	0.79
Stone Displacement	0.89	1.00	0.68
Stone Velocity	0.79	0.68	1.00

3.6. Flow Reversal and Local Reflux Phenomena

A key finding of the simulations is the local flow reversal (reflux) at certain stages of the peristaltic cycle. Table 4 measures this effect by showing both the minimum reverse velocity in the domain at each time instant and the region where reflux is most conspicuous. The results of Table 4 indicate that the flow reversal can be observed at any stage of the peristaltic cycle except the starting point. The maximum reverse velocity rises to -0.32 x 10^{-4} m/s at 2 s and to -3.12 x 10^{-4} m/s at 8 s, showing that the reflux is more intense at time 8 s when the wave cycles interact with the stone more than at time 2 s. Interestingly, however, the direction of the reflux changes with the phase of the peristaltic wave. Reflux is mainly apparent during the wave contraction phases (t = 2-6 s) when the flow is divided downstream of the stone to form a recirculation bubble. The reflux may also be done between the stone and upstream during the relaxation stages of the waves (t = 8 s) as the pressure gradient is reversed temporarily. Reflux episodes last between 0.41 and 0.72 seconds, which is a substantial fraction of each peristaltic cycle. This result has significant clinical implications due to the possibility of bacteria or stone micro-fragments being brought back to the kidney by reflux, which may pose an increased risk of infection or result in more difficult stone clearance.

Table 4.
Analysis of local flow reversal (reflux) during the peristaltic cycle.

Time (s)	Max Reverse Velocity ($\times 10^{-4}$ m/s)	Reflux Region	Duration of Reflux (s)
0	0.00	None	0.00
2	-0.32	Downstream of the stone	0.41
4	-1.78	Downstream of the stone	0.63
6	-2.45	Downstream of the stone	0.58
8	-3.12	Upstream of the stone	0.72
10	-1.89	Downstream of the stone	0.49

3.7. Wall Shear Stress Distribution

Wall shear stress (WSS) is a very important parameter to be aware of the mechanical forces acting on the ureteral epithelium. The high level of WSS may possibly lead to tissue damage or trigger biological reactions. Table 5 shows the maximum values of shear stress at each time moment and their locations along the ureter. At t = 0 s, the stress associated with the base wall is 0.042 Pa, which is within the expected range of low velocity internal flow. When the peristaltic wave travels and responds to the stone, WSS dramatically rises to 0.423 Pa at t = 6 s - more than 10 times the starting level. This large amplification is in the narrow gap between the stones, where high-velocity gradients form. The increase in the WSS carries on into the simulation, with the values being 7-10 times greater than the baseline, even during the relaxation phases of the waves. This long-term increase indicates that the existence of a stone produces a chronic mechanical stressful environment that can have consequences for the health of ureteral tissue. The spatial distribution of WSS (which was earlier depicted in Figures 5 and was confirmed with Najafi et al. [11] indicates that the maximum shear stress is encountered just a bit upstream of the maximum diameter of the stone, with the acceleration of the flow being the most effective. This effect of localized stress concentration may have a possible impact on stone erosion or fragmentation over longer time periods.

Table 5.
Maximum wall shear stress and its location over time.

Time (s)	Max WSS (Pa)	Location of Max WSS	Relative to Baseline
0	0.042	Inlet region	1.0×
2	0.187	Stone vicinity	4.5×
4	0.356	Stone vicinity	8.5×
6	0.423	Stone vicinity	10.1×
8	0.298	Stone vicinity	7.1×
10	0.401	Stone vicinity	9.5×

3.8. Energy Considerations and Pumping Efficiency

To evaluate the efficiency of the entire peristaltic pumping mechanism under the influence of an obstruction, Table 6 shows the energy analysis of the pressure forces work on the fluid and stone transportation. This pressure work done by the fluid ranges between 1.24 μJ in the first interval and a peak of 3.56 μJ in the 4-6 s range, which is the range of maximum peristaltic contraction. The final pressure work during the 10-second simulation is 13.70 μJ. This energy is imparted to the stone in 2 forms, namely kinetic energy (because it is moving) and potential energy (because of its motion relative to the opposing pressure field). The gain in kinetic energy is quite low (0.0807 μJ) since the stone is moving slowly, whereas the potential energy gain (1.4457 μJ) is the largest contribution to the amount of work done on the stone. The pumping efficiency is the ratio of the total energy acquired by the stone to the pressure work acquired by the fluid, and it has an average of 10.55% through the simulation. This comparatively low efficiency means that the majority of the energy of the fluid is wasted in viscous losses or is utilized to keep the fluid flowing instead of directly driving the stone. The highest efficiency is 12.33% at the strongest contraction phase (4-6 s), which indicates that synchronized timing of waves may have the potential to maximize the transport of the stones.

Table 6.
Energy analysis of peristaltic pumping with obstruction.

Time Interval (s)	Pressure Work (μJ)	Stone Kinetic Energy Gain (μJ)	Stone Potential Energy Gain (μJ)	Pumping Efficiency (%)
0-2	1.24	0.008	0.112	9.68
2-4	2.87	0.021	0.298	11.12
4-6	3.56	0.027	0.412	12.33
6-8	2.91	0.015	0.289	10.45
8-10	3.12	0.009	0.334	10.99
Total/Cumulative	13.70	0.080	1.445	10.55 (avg)

3.9. Summary of Key Findings

Quantitative findings of this section offer a number of significant clues to the mechanisms of peristaltic urine flow in the presence of a kidney stone:

- Pressure pulsation generated by peristaltic waves creates a fluctuating pressure difference across the stone, with amplitudes reaching up to 8.37 Pa.
- Stone migration occurs progressively over multiple wave cycles, with a net displacement of 3.354 mm observed over 10 seconds of simulation.
- Local reflux episodes occur during each wave cycle, with reverse velocities up to -3.12×10^{-4} m/s, potentially contributing to retrograde transport of bacteria or debris.
- Wall shear stress increases dramatically (up to 10-fold) in the vicinity of the stone, creating a sustained mechanical loading environment that may have biological implications.
- Pumping efficiency for stone transport is approximately 10-12%, indicating that most fluid energy is dissipated rather than used for stone propulsion.

All these results prove that although peristaltic waves can produce strong propulsive forces and move stones slowly towards the bladder, it is an inefficient process that is not without complicated flow effects such as reflux and high wall shear stress. These aspects can affect the natural history of the stone disease and the reaction to the therapeutic treatment.

4. Conclusion

In this study, a comprehensive two-dimensional axisymmetric numerical model was developed to investigate the dynamics of peristaltic urine flow in a human ureter obstructed by a mobile kidney stone. The simulations incorporated two-way fluid-structure interaction between the urine, the deformable ureteral wall undergoing sinusoidal peristaltic motion, and a rigid stone free to translate axially under hydrodynamic forces. The model was validated against published data, showing excellent agreement in pressure distribution and wall shear stress profiles. The results demonstrate that peristaltic waves generate significant pressure pulsations across the obstructing stone, with pressure differentials reaching 8.37 Pa during peak contraction. This pressure difference serves as the primary driving mechanism for stone transport, producing cumulative stone displacement of 3.354 mm toward the bladder over 10 seconds of simulated time. The strong correlation (0.89) between pressure differential and stone displacement confirms the dominance of pressure-driven transport.

Flow acceleration in the narrow annular gap between the stone and ureteral wall increases maximum fluid velocity nearly seven-fold compared to baseline, reaching 5.99×10^{-3} m/s. This acceleration generates dramatically elevated wall shear stress in the stone vicinity, with values up to ten times baseline (0.423 Pa versus 0.042 Pa). Such sustained mechanical loading may have significant implications for ureteral tissue health, potentially contributing to inflammation or tissue remodeling in patients with chronic stone disease. An important finding is the occurrence of local flow reversal (reflux) during each peristaltic cycle, with reverse velocities up to -3.12×10^{-4} m/s persisting for 0.41-0.72 seconds. The location of reflux shifts between downstream of the stone during contraction phases and upstream during relaxation phases. This phenomenon has clinical significance, as reflux could potentially transport bacteria or stone micro-fragments back toward the kidney, increasing infection risk or complicating stone clearance. Energy analysis reveals that peristaltic pumping for stone transport is relatively inefficient, with only 10.55% of fluid pressure work converted to stone kinetic and potential energy. The majority of fluid energy is dissipated through viscous losses, with efficiency peaking at 12.33% during maximum contraction. This suggests that while peristalsis can gradually move stones, the process is inherently dissipative.

Several limitations of the present study should be acknowledged. The axisymmetric geometry, while computationally efficient, cannot capture three-dimensional asymmetries in stone shape or ureteral lumen. The linear elastic wall model neglects the nonlinear and viscoelastic properties of biological tissue. The stone is assumed to be perfectly spherical and smooth, whereas actual renal calculi exhibit irregular morphology. No mechanical contact or friction between the stone and wall is considered, which may become important as the stone approaches the wall. Additionally, the simulations are limited to 10 seconds, representing only a few peristaltic cycles.

Future work should extend the model to three dimensions with realistic lumen geometries derived from medical imaging. Incorporation of hyperelastic and viscoelastic material models for the ureteral wall would improve physiological accuracy. Non-Newtonian fluid models for urine should be considered, as urine exhibits shear-thinning behavior. Mechanical contact algorithms could capture stone-wall interactions during complete obstruction. Longer simulation times would reveal stone transport over clinically relevant time scales. In conclusion, this study provides quantitative insights into the hydrodynamic environment of the obstructed ureter and the forces governing kidney stone transport. The findings enhance understanding of stone disease pathophysiology and may inform clinical decisions regarding spontaneous passage versus intervention, as well as the design of medical devices such as ureteral stents. The demonstrated occurrence of reflux and elevated wall shear stress highlights potential mechanical factors contributing to ureteral tissue damage and infection risk, suggesting avenues for future research and therapeutic development.

Transparency:

The authors confirm that the manuscript is an honest, accurate, and transparent account of the study; that no vital features of the study have been omitted; and that any discrepancies from the study as planned have been explained. This study followed all ethical practices during writing.

Copyright:

References

[1] F. Kiil, "Function of the ureter and renal pelvis," *Annals of Surgery*, vol. 148, no. 2, pp. 280-291, 1958.

[2] D. J. Griffiths and C. Notschaele, "The mechanics of urine transport in the upper urinary tract: 1. The dynamics of the isolated bolus," *Neurourology and Urodynamics*, vol. 2, no. 2, pp. 155-166, 1983. https://doi.org/10.1002/nau.1930020209

[3] A. R. Crowley, J. C. Byrne, E. D. Vaughan Jr, and D. N. Marion, "The effect of acute obstruction on ureteral function," *The Journal of Urology*, vol. 143, no. 3, pp. 596-599, 1990. https://doi.org/10.1016/S0022-5347(17)40037-1

[4] D. Carugo, M. ElMahdy, X. Zhao, M. J. Drake, X. Zhang, and F. Clavica, "An artificial model for studying fluid dynamics in the obstructed and stented ureter," in *Proceedings of the 35th Annual International Conference of the IEEE Engineering in Medicine and Biology Society (EMBC) (pp. 5335–5338). Osaka, Japan: IEEE*, 2013.

[5] Y.-C. B. Fung, *Peristaltic pumping: A bioengineering model. In S. Boyarsky, C. W. Gottschalk, E. A. Tanagho, & P. D. Zimskind (Eds.), Urodynamics: Hydrodynamics of the ureter and renal pelvis.* New York: Elsevier, 1971.

[6] B. R. Kumar and K. Naidu, "A numerical study of peristaltic flows," *Computers & Fluids*, vol. 24, no. 2, pp. 161-176, 1995. https://doi.org/10.1016/0045-7930(94)00027-V

[7] B. Vahidi and N. Fatouraee, "A biomechanical simulation of ureteral flow during peristalsis using intraluminal morphometric data," *Journal of Theoretical Biology*, vol. 298, pp. 42-50, 2012. https://doi.org/10.1016/j.jtbi.2011.12.019

[8] G. Hosseini, J. Williams, E. J. Avital, A. Munjiza, D. Xu, and J. A. Green, "Computational simulation of urinary system," in *San Francisco, USA: Proc World Congress Eng Comput Sci*, 2012.

[9] G. Hosseini *et al.*, "A computational model of ureteral peristalsis and an investigation into ureteral reflux," *Biomedical Engineering Letters*, vol. 8, pp. 117-125, 2018. https://doi.org/10.1007/s13534-017-0053-0

[10] Z. Najafi, P. Gautam, B. F. Schwartz, A. J. Chandy, and A. M. Mahajan, "Three-dimensional numerical simulations of peristaltic contractions in obstructed ureter flows," *Journal of Biomechanical Engineering*, vol. 138, no. 10, p. 101002, 2016. https://doi.org/10.1115/1.4034307

[11] Z. Najafi, B. Schwartz, A. Chandy, and A. Mahajan, "A two-dimensional numerical study of peristaltic contractions in obstructed ureter flows," *Computer Methods in Biomechanics and Biomedical Engineering*, vol. 21, no. 1, pp. 22-32, 2018. https://doi.org/10.1080/10255842.2017.1415333

[12] A. T. Takaddus and A. J. Chandy, "A three-dimensional (3D) two-way coupled fluid-structure interaction (FSI) study of peristaltic flow in obstructed ureters," *International Journal for Numerical Methods in Biomedical Engineering*, vol. 34, no. 10, p. e3122, 2018. https://doi.org/10.1002/cnm.3122

[13] S. Abbasian and R. Maddahian, "Numerical analysis of an obstacle motion in the human ureter using the dynamic mesh approach," *International Journal for Numerical Methods in Biomedical Engineering*, vol. 40, no. 3, p. e3800, 2024. https://doi.org/10.1002/cnm.3800

[14] L. G. Keni *et al.*, "Computational flow analysis of a single peristaltic wave propagation in the ureter," *Computer Methods and Programs in Biomedicine*, vol. 210, p. 106378, 2021. https://doi.org/10.1016/j.cmpb.2021.106378

[15] J. Jiménez-Lozano, M. Sen, and E. Corona, "Analysis of peristaltic two-phase flow with application to ureteral biomechanics," *Acta Mechanica*, vol. 219, no. 1, pp. 91-109, 2011. https://doi.org/10.1007/s00707-010-0438-y

[16] T. Adibi, O. Adibi, and S. E. Razavi, "A characteristic-based solution of forced and free convection in closed domains with emphasis on various fluids," *International Journal of Engineering*, vol. 32, no. 11, pp. 1689-1695, 2019. https://doi.org/10.5829/ije.2019.32.11b.20

[17] T. Adibi, S. E. Razavi, S. F. Ahmed, H. Hassanpour, N. Mohammadzadeh, and S. M. Muyeen, "Fluid-Structure-Acoustic coupling analysis for external laminar and turbulent fluid flows," *Results in Physics*, vol. 49, p. 106496, 2023. https://doi.org/10.1016/j.rinp.2023.106496